NASA Technical Memorandum 100412

Preliminary In-Flight Boundary Layer Transition Measurements on a 45-Degree Swept Wing at Mach Numbers Between 0.9 and 1.8

J. Blair Johnson

March 1988

National Aeronautics and
Space Administration

NASA Technical Memorandum 100412

Preliminary In-Flight Boundary Layer Transition Measurements on a 45-Degree Swept Wing at Mach Numbers Between 0.9 and 1.8

J. Blair Johnson
Ames Research Center, Dryden Flight Research Facility, Edwards, California

1988

National Aeronautics and
Space Administration
Ames Research Center
Dryden Flight Research Facility
Edwards, California 93523-5000

CONTENTS

	Page
SUMMARY	1
INTRODUCTION	1
NOMENCLATURE	2
DESCRIPTION OF TEST AIRCRAFT AND WING MODIFICATION	3
INSTRUMENTATION	4
FLOW VISUALIZATION	4
TEST CONDITIONS AND MANEUVERS	5
RESULTS AND DISCUSSION	5
Typical Pressure Distributions	5
Typical Transition Results	5
CONCLUDING REMARKS	7
APPENDIX — TABULATED PRESSURE COEFFICIENTS	8
REFERENCES	22
TABLES	23
FIGURES	27

SUMMARY

A preliminary flight experiment was flown to generate a full-scale supersonic data base to aid the assessment of computational codes, to improve instrumentation for measuring boundary layer transition at supersonic speeds, and to provide preliminary information for the definition of follow-on programs. The experiment was conducted using an F-15 aircraft that was modified with a small cleanup test section on the right wing. Results are presented for Mach (M) numbers from 0.9 to 1.8 at altitudes from 26,000 to 55,000 ft. They were combined to give a unit Reynolds number range of 1.7 to 4.0 million per ft. Angle of attack varied from approximately -1° to 10°.

At $M \geq 1.2$, transition occurred near or at the leading edge for the clean configuration. The furthest aft that transition was measured was 20 percent chord at $M = 0.9$ and $M = 0.97$. No change in transition location was observed after the addition of a notch-bump on the leading edge of the inboard side of the test section which was intended to minimize attachment line transition problems.

Some flow visualization was attempted during the flight experiment with both subliming chemicals and liquid crystals. However, difficulties arose from the limited time the test aircraft was able to hold test conditions and the difficulty of positioning the photo chase aircraft during supersonic test points. Therefore, no supersonic transition results were obtained using flow visualization.

INTRODUCTION

Recently, there has been a renewed interest in the feasibility of obtaining significant amounts of laminar flow at supersonic speeds. Although some supersonic boundary layer transition work was done on wings in the late 1950s (Banner and others, 1958; McTigue and others, 1959) and on the Arnold Engineering Development Center 10°-transition cone (Fisher and Dougherty, 1982), the most recent and extensive boundary layer transition work on lifting surfaces has concentrated on the transonic speed region (Runyan and others, 1984; Meyer and others, 1987). In addition, the development and increased sophistication of computational codes have led to a need for a large full-scale experimental data base to validate these codes.

Consequently, the NASA Ames-Dryden Flight Research Facility at Edwards, California conducted a preliminary flight experiment during the winter and spring of 1986 using an F-15 aircraft. The objectives of the flight experiment were to generate a full-scale supersonic data base for assessing computational tools, to improve instrumentation for measuring boundary layer transition at supersonic speeds, and to provide information for the definition of follow-on programs.

The flight experiment examined Mach numbers ranging from 0.9 to 1.8 and altitudes from 26,000 to 55,000 ft to give a range of unit Reynolds numbers from 1.7 to 4.0 million per ft. Angle of attack was varied from -1° to approximately 10°.

NOMENCLATURE

ALPHA	angle of attack, deg
BETA	angle of sideslip, deg
BL	butt line, in.
c	airfoil chord, ft
Cp	pressure coefficient (PL-PSINF)/QBAR
Hp	pressure altitude, ft
IB	inboard row of pressure orifices
L.S.	lower surface
M	Mach number
MINF	free-stream Mach number
OB	outboard row of pressure orifices
PL	local static pressure, lb/ft^2
PSINF	free-stream static pressure, lb/ft^2
QBAR	dynamic pressure, lb/ft^2
Rn	Reynolds number based on free-stream conditions and local chord
Rn t	transition Reynolds number
U.S.	upper surface
x	longitudinal dimension, in.
x/c	nondimensional chord location
x/c t	nondimensional chord location of transition
y	lateral dimension, in.
z	vertical dimension, in.
z/c	nondimensional vertical location

DESCRIPTION OF TEST AIRCRAFT AND WING MODIFICATION

The flight experiment was conducted using an F-15 twin-engine fighter aircraft. The F-15 airplane was chosen for the experiment primarily because of its Mach 2 capability and availability. In addition, previous flight experiments on the F-15 airplane showed that the wing produced a favorable pressure gradient (desirable for obtaining laminar flow) to approximately 25 percent chord. The F-15 aircraft has 45° of leading edge sweep and uses a NACA 64(A)04.6 airfoil at BL 155. Airfoil coordinates at several butt lines are given in table 1. These values do not include the thickness of the wing modification.

A foam and fiberglass cleanup test section was placed on the right wing of the aircraft. Figure 1 shows an in-flight photograph of the F-15 airplane with the foam and fiberglass test section. This near planform view shows the relative location and size of the test section. The intended purpose of the foam and fiberglass test section was to eliminate any possible effects of surface roughness or imperfections. It retained the existing airfoil shape but added approximately 3/16 to 1/4 in. of thickness. This thickness was necessary for the installation of instrumentation plumbing lines. The test section was approximately 4 ft wide, the inboard edge at BL 170 and the outboard edge at BL 218. The aft edge of the test section extended to approximately 30 percent chord on the inboard side and approximately 35 percent chord on the outboard side. The drawing in figure 2 shows the exact location of the test section and the chord values for the inboard and outboard edges of the test section. It had two rows of 15 flush static pressure orifices, one at BL 176, the other at BL 212. The exact chord location of the orifices is given in table 2.

The test section was constructed using one layer of unidirectional fiberglass under 1/8 in. polyurethane foam covered with four layers of bidirectional fiberglass. The surface consisted of body putty and polyester paint. A cross-sectional drawing of the test section is given in figure 3. The waviness of the test section did not exceed 0.0015 in. per 2 in. It was originally painted white but was repainted black towards the end of the experiment to facilitate the use of liquid crystals for flow visualization. In addition, a notch-bump was added to the inboard side of the test section after the sixth flight to eliminate any possible effects of an attachment line transition problem (Gaster, 1965). A photograph of the notch-bump is shown in figure 4.

A potential problem with this construction technique for high altitude and supersonic use was observed after several test flights. Small blisters of approximately 1/16 to 1/8 in. in diameter and approximately 0.002 to 0.010 in. high began to appear in the paint after a flight in which the maximum Mach and altitude were 1.8 and 50,000 ft, respectively. Although the blisters did not break the surface of the paint, they presented an obvious problem for using this construction technique at Mach (M) numbers near 2.0 and above for laminar flow testing. The blisters were caused by gas that was released as the test section was exposed to the higher temperatures caused by flying at supersonic speeds. The origin of the gas is uncertain, but it may have been trapped in the body putty during construction or formed by the resin material during high-temperature exposure. In addition, altitude was considered to aid in the formation of the blisters because of the reduced pressure at altitude resulting in a substantial pressure differential between the trapped gas and the atmosphere.

INSTRUMENTATION

Two separate instrumentation systems were used for the flight experiment. Quantities such as free-stream Mach number, pressure altitude, and angle of attack were obtained from the aircraft's main instrumentation system. The main system used two absolute pressure transducers for measuring total and static pressure from the flight test pitot-static probe mounted on a noseboom.

The instrumentation system for the test section consisted of a 32-port, electronically scanned, multiple differential pressure transducer unit, an absolute pressure transducer, and five temperature-compensated hot-film anemometers. The differential pressure transducer unit was used to measure pressures from the two rows of static pressure orifices. The absolute pressure transducer measured the pressure on the reference side of the differential pressure transducer unit. The temperature-compensated hot-film anemometers, similar to the system described in Chiles and Johnson (1985), were used to measure transition location. Temperature-compensated hot-film anemometers were used because changes in ambient, wall, or total temperature can affect the output signal quality of uncompensated hot-film anemometers. The hot-film sensors had a nominal resistance of 12 ohms and the temperature gages had a nominal resistance of 50 ohms. Figure 5 shows a closeup of the hot-film sensor and temperature gage as installed on the test section.

Because only five hot-film anemometers were available on the aircraft, they were relocated from flight to flight to accurately define transition location. The chord locations of the hot film for the various flights of the experiment are given in table 3. The hot-film sensors remained in the 1, 2, 4, 10, and 15 percent chord locations for the entire latter portion of the experiment. Figure 6 shows the hot-film sensors mounted on the test section at 5, 10, 15, 20, and 15 percent chord.

FLOW VISUALIZATION

At several times during the flight test program, attempts were made to use flow visualization as a secondary means of determining transition location. Although no flow visualization results are given, a discussion of the effort is provided to aid future development of flow visualization techniques for supersonic flight. Initially, a mixture of napthalene and red food coloring was used. The red food coloring was added to give greater contrast between the white test section and the napthalene. Only two flights were flown before the napthalene was abandoned because of operational difficulties. The difficulties arose from trying to apply the correct amount of napthalene that would not sublime during the climb and acceleration, but would sublime during the short amount of time (approximately 10 to 20 sec) on test conditions that followed.

After the early portion of flight tests, the test section was painted black to facilitate the use of liquid crystals similar to the technique used in Holmes and others (1986). Pressure sensitive liquid crystals (named by the manufacturer) were used. Operational difficulties were still encountered, however. It was extremely difficult to get the photo chase aircraft in the desired position during supersonic

test runs and was virtually impossible during test points where the test aircraft was in a turn. Because of these difficulties, liquid crystal photos were taken only at low-transonic speeds. An obvious solution would have been to mount a camera on the test aircraft. However, this would have entailed extensive modifications beyond the scope of the project.

TEST CONDITIONS AND MANEUVERS

Test points were flown at Mach numbers ranging between 0.9 and 1.8 at altitudes between 26,000 and 55,000 ft. Mach number and altitude were combined to give a unit Reynolds number range from 1.7 to 4.0 million per ft. Angle of attack ranged from -1° to 10°.

Straight and level points were flown for approximately 20 sec. In order to vary angle of attack, constant g-loading turns were flown. Each constant g-loading condition was held for approximately 10 sec. At the higher Mach numbers and increased g-loading, it was often difficult to maintain both airspeed and altitude, therefore airspeed was given the higher priority. This resulted in some cases where altitude was allowed to decrease to maintain airspeed.

RESULTS AND DISCUSSION

Typical Pressure Distributions

Typical pressure distributions for M = 0.9, 1.2, 1.5, and 1.8 are shown in figure 7. Except for the inboard row at M = 0.9, the pressure distributions show a favorable gradient to approximately 20 percent chord, or greater, for the inboard pressure orifice row. The outboard row indicates a favorable pressure gradient, at least to the aft most orifice, of 33 percent, except for the lower angle-of-attack case at M = 0.9 where the slope became negative near 20 percent chord. An increase in angle of attack increased the pressure measured at the two lower surface orifices as would be expected and decreased the pressure on the upper surface of the test section. At the lower speed cases, M = 0.9 and 1.2, increased angle of attack had a noticeable effect on the shape of the forward portion of the pressure distribution.

These pressure distributions are presented for the typical case. Tabulated pressure coefficients are presented in the appendix for Mach numbers at angles of attack ranging from 1° to 7° but categorized by unit Reynolds numbers of approximately 1.7 and 2.0 million per ft for both the clean and notch-bump configuration. Tabulated pressure coefficients for the higher Reynolds number cases where no laminar flow was detected are not given.

Typical Transition Results

The output from the hot-film anemometers was used to determine boundary layer transition. Figure 8 shows typical outputs from the five anemometers during a test

point at M = 0.9, Hp = 40,600 ft. In figure 8(a) where the angle of attack is 3.3°, the hot-film sensor at 5 percent chord shows an output typical of transitional flow. The other outputs (10, 15, and 20 percent) demonstrate signals typical of turbulent flow. The amplitude of the output for the 10 percent chord anemometer is less than the others, for the same flow condition, because the gain of that particular anemometer was inadvertently set low for several flights.

In figure 8(b) where the angle of attack is 5.0°, the hot films at 5 and 10 percent chord indicate laminar flow. The two gages at 15 percent chord indicate laminar flow with turbulent spikes, and the gage at 20 percent chord indicates periods of transitional flow and turbulent flow with laminar spikes.

At M $\geq$ 1.2, transition occurred at or very near the leading edge. Figure 9 shows a typical hot-film output for Mach numbers > 1.2. The flight conditions for this point were M = 1.73, Hp = 49,200, ALPHA = 4.5°. All the hot-film gages indicate turbulent flow. Again, the gain on the 10 percent chord hot film was set lower than the others, thus giving the lower amplitude signal. In addition, the inboard 15 percent chord hot film failed early in the flight and was inoperative for this test point. Overall, the temperature-compensated hot-film anemometers worked well for determining transition location throughout the Mach-number range of the experiment.

Summary plots of the most aft that transition occurred, or optimum transition location, are given in figures 10 and 11. Figure 10 presents a plot of optimum transition location as a function of angle of attack for the clean leading-edge configuration at M = 0.9. For this Mach number, the longest runs of laminar flow occurred at 5° and 6° angle of attack. Above 6° and below 5° angle of attack, transition occurred at 5 percent chord or less.

Figure 11 presents optimum transition location as a function of free-stream Mach number for both the clean and notch-bump configurations. Transition occurred at 20 percent chord at M = 0.9 and M = 0.97 for the clean configuration. For the notch-bump configuration at M = 0.9, transition occurred at approximately 15 percent chord. It is important to note that even though the 15 percent chord hot film never indicated pure laminar flow, there were no hot-film gages aft of 15 percent chord to accurately determine transition location. At M = 1.10 (clean configuration) and M = 1.16 (notch-bump configuration), transition occurred at 15 percent chord. At M $\geq$ 1.2, transition occurred near the leading edge for both leading-edge configurations. It is apparent that the notch-bump had essentially no effect.

The cause of the sharp decrease in optimum transition location and the inability to obtain laminar flow at M > 1.2 is uncertain. But it is important to mention that at the higher Mach numbers (M = 1.2, 1.5, and 1.8), the same angle-of-attack range as at the slower speeds was achieved, therefore eliminating angle of attack as a possibility.

Figure 12 presents transition Reynolds number, based on the optimum transition location, as a function of Mach number. The M = 1.16 test point was obtained with the notch-bump on the leading edge. Transition Reynolds numbers for the optimum cases decreased from approximately 4 million per ft at M = 0.9 to 2 million at M = 1.1 and then increased to 3 million at M = 1.16.

CONCLUDING REMARKS

A preliminary flight experiment was flown to generate a full-scale data base to aid with the assessment of computational codes and improve instrumentation and techniques for measuring boundary layer transition at supersonic speeds.

1. Temperature-compensated hot films worked extremely well for measuring boundary layer transition throughout the Mach range of the experiment.

2. The limit of the foam and fiberglass technique for constructing cleanup test sections or contouring desired airfoils for boundary layer transition experiments appears to be approximately M = 1.8 and Hp = 50,000 ft because of the occurrence of surface blisters which spoil the original smooth surface.

3. Transition was measured as far aft as 20 percent chord at M = 0.90 and M = 0.97. At M = 1.10 and M = 1.16, transition was measured at 15 percent chord. At M > 1.20, transition occurred near the leading edge. Maximum observed transition Reynolds number for this experiment, NACA 64(A)04.6 airfoil with 45° leading-edge sweep, was approximately 4 million per ft.

4. There was no change in optimum transition location (limited to a resolution of 5 percent chord in some cases) with the addition of a notch-bump on the leading edge of the test section.

Ames Research Center
Dryden Flight Research Facility
National Aeronautics and Space Administration
Edwards, California, August 20, 1987.

APPENDIX — TABULATED PRESSURE COEFFICIENTS

Mach (M) = 0.900 Pressure altitude, ft (Hp) = 40,637
Angle of attack, deg (α) = 3.34 L.S. = lower surface U.S. = upper surface
x/c = nondimensional chord location

Inboard row

	x/c, %	
L.S.	1.3	-0.008
	0.86	-0.023
	0	Inoperative
U.S.	0.73	-0.341
	1.20	-0.458
	3.30	-0.606
	6.20	-0.647
	8.20	-0.589
	10.20	-0.654
	12.60	-0.715
	15.10	-0.783
	17.50	-0.852
	20.10	-0.635
	25.00	-0.488
	29.80	-0.682

Outboard row

	x/c, %	
L.S.	1.50	-0.309
	1.00	-0.335
	0	0.381
U.S.	1.00	-0.238
	1.40	-0.342
	3.60	-0.448
	7.00	-0.586
	9.10	-0.625
	11.30	-0.634
	14.00	-0.677
	16.80	-0.711
	19.60	-0.762
	22.40	Inoperative
	22.70	-0.624
	33.00	-0.676

M = 0.897 Hp = 40,580 α = 4.95

Inboard row

	x/c, %	
L.S.	1.3	0.072
	0.86	0.199
	0	Inoperative
U.S.	0.73	-0.763
	1.20	-0.823
	3.30	-0.939
	6.20	-0.975
	8.20	-0.972
	10.20	-1.028
	12.60	-1.064
	15.10	-1.076
	17.50	-1.082
	20.10	-1.041
	25.00	-1.030
	29.80	-0.908

Outboard row

	x/c, %	
L.S.	1.50	-0.043
	1.00	0.004
	0	0.051
U.S.	1.00	-0.644
	1.40	-0.712
	3.60	-0.837
	7.00	-0.901
	9.10	-0.921
	11.30	-0.974
	14.00	-0.991
	16.80	-0.998
	19.60	-1.022
	22.40	Inoperative
	22.70	-1.066
	33.00	-1.127

M= 0.910 Hp = 38,101 α = 2.09

Inboard row

	x/c, %	
L.S.	1.3	-0.269
	0.86	-0.364
	0	Inoperative
U.S.	0.73	-0.141
	1.20	-0.247
	3.30	-0.393
	6.20	-0.514
	8.20	-0.586
	10.20	-0.538
	12.60	-0.487
	15.10	-0.500
	17.50	-0.524
	20.10	-0.542
	25.00	-0.500
	29.80	-0.632

Outboard row

	x/c, %	
L.S.	1.50	-0.719
	1.00	-0.729
	0	0.330
U.S.	1.00	-0.066
	1.40	-0.146
	3.60	-0.292
	7.00	-0.447
	9.10	-0.495
	11.30	-0.523
	14.00	-0.561
	16.80	-0.598
	19.60	-0.557
	22.40	Inoperative
	22.70	-0.543
	33.00	-0.637

M = 0.916 Hp = 37,221 α = 5.47

Inboard row

	x/c, %	
L.S.	1.3	0.202
	0.86	0.245
	0	Inoperative
U.S.	0.73	-0.756
	1.20	-0.797
	3.30	-0.939
	6.20	-0.939
	8.20	-0.947
	10.20	-0.980
	12.60	-1.015
	15.10	-1.064
	17.50	-1.087
	20.10	-1.041
	25.00	-0.988
	29.80	-1.146

Outboard row

	x/c, %	
L.S.	1.50	0.041
	1.00	0.059
	0	0.037
U.S.	1.00	-0.640
	1.40	-0.724
	3.60	-0.835
	7.00	-0.872
	9.10	-0.947
	11.30	-0.940
	14.00	-0.965
	16.80	-0.988
	19.60	-1.026
	22.40	Inoperative
	22.70	-1.052
	33.00	-1.089

M = 1.186 Hp = 45,876 α = 2.00

Inboard row

	x/c, %	
L.S.	1.3	-0.382
	0.86	-0.417
	0	Inoperative
U.S.	0.73	0.136
	1.20	0.049
	3.30	-0.098
	6.20	-0.202
	8.20	-0.220
	10.20	-0.268
	12.60	-0.302
	15.10	-0.373
	17.50	-0.446
	20.10	-0.415
	25.00	-0.385
	29.80	-0.431

Outboard row

	x/c, %	
L.S.	1.50	-0.570
	1.00	-0.578
	0	0.452
U.S.	1.00	0.200
	1.40	0.144
	3.60	-0.004
	7.00	-0.125
	9.10	-0.180
	11.30	-0.245
	14.00	-0.260
	16.80	-0.317
	19.60	-0.328
	22.40	Inoperative
	22.70	-0.377
	33.00	-0.427

M = 1.198 Hp = 45,638 α = 6.35

Inboard row

	x/c, %	
L.S.	1.3	0.203
	0.86	0.200
	0	Inoperative
U.S.	0.73	-0.193
	1.20	-0.261
	3.30	-0.384
	6.20	-0.449
	8.20	-0.481
	10.20	-0.504
	12.60	-0.547
	15.10	-0.565
	17.50	-0.623
	20.10	-0.582
	25.00	-0.561
	29.80	-0.674

Outboard row

	x/c, %	
L.S.	1.50	-0.077
	1.00	-0.102
	0	0.406
U.S.	1.00	-0.102
	1.40	-0.171
	3.60	-0.288
	7.00	-0.358
	9.10	-0.421
	11.30	-0.457
	14.00	-0.476
	16.80	-0.517
	19.60	-0.514
	22.40	Inoperative
	22.70	-0.582
	33.00	-0.620

M = 1.210 Hp = 41,891 α = 1.42

Inboard row

	x/c, %	
L.S.	1.3	-0.412
	0.86	-0.480
	0	Inoperative
U.S.	0.73	0.194
	1.20	0.109
	3.30	-0.043
	6.20	-0.133
	8.20	-0.187
	10.20	-0.230
	12.60	-0.271
	15.10	-0.333
	17.50	-0.366
	20.10	-0.351
	25.00	-0.347
	29.80	-0.364

Outboard row

	x/c, %	
L.S.	1.50	-0.604
	1.00	-0.600
	0	0.438
U.S.	1.00	0.235
	1.40	0.188
	3.60	0.062
	7.00	-0.078
	9.10	-0.146
	11.30	-0.183
	14.00	-0.224
	16.80	-0.287
	19.60	-0.287
	22.40	Inoperative
	22.70	-0.335
	33.00	-0.385

M = 1.212 Hp = 41,536 α = 4.95

Inboard row

	x/c, %	
L.S.	1.3	0.125
	0.86	0.088
	0	Inoperative
U.S.	0.73	-0.058
	1.20	-0.134
	3.30	-0.252
	6.20	-0.341
	8.20	-0.399
	10.20	-0.400
	12.60	-0.452
	15.10	-0.501
	17.50	-0.472
	20.10	-0.504
	25.00	-0.512
	29.80	-0.602

Outboard row

	x/c, %	
L.S.	1.50	-0.193
	1.00	-0.359
	0	0.476
U.S.	1.00	0.038
	1.40	0.002
	3.60	-0.147
	7.00	-0.255
	9.10	-0.319
	11.30	-0.353
	14.00	-0.386
	16.80	-0.424
	19.60	-0.404
	22.40	Inoperative
	22.70	-0.500
	33.00	-0.516

M = 1.501 Hp = 50,924 α = 2.02

Inboard row

	x/c, %	
L.S.	1.3	-0.180
	0.86	-0.231
	0	Inoperative
U.S.	0.73	0.268
	1.20	0.206
	3.30	0.062
	6.20	-0.025
	8.20	-0.072
	10.20	-0.087
	12.60	-0.133
	15.10	-0.183
	17.50	-0.224
	20.10	-0.245
	25.00	-0.231
	29.80	-0.277

Outboard row

	x/c, %	
L.S.	1.50	-0.202
	1.00	-0.208
	0	0.537
U.S.	1.00	0.328
	1.40	0.271
	3.60	0.155
	7.00	0.043
	9.10	-0.016
	11.30	-0.052
	14.00	-0.103
	16.80	-0.135
	19.60	-0.152
	22.40	Inoperative
	22.70	-0.197
	33.00	-0.232

M = 1.442 Hp = 50,965 α = 6.94

Inboard row

	x/c, %	
L.S.	1.3	0.315
	0.86	0.312
	0	Inoperative
U.S.	0.73	-0.024
	1.20	-0.088
	3.30	-0.174
	6.20	-0.240
	8.20	-0.281
	10.20	-0.296
	12.60	-0.330
	15.10	-0.365
	17.50	-0.392
	20.10	-0.400
	25.00	-0.355
	29.80	-0.441

Outboard row

	x/c, %	
L.S.	1.50	0.147
	1.00	0.032
	0	0.511
U.S.	1.00	0.067
	1.40	-0.009
	3.60	-0.092
	7.00	-0.165
	9.10	-0.221
	11.30	-0.237
	14.00	-0.270
	16.80	-0.297
	19.60	-0.325
	22.40	Inoperative
	22.70	-0.360
	33.00	-0.383

M = 1.495 Hp = 46,858 α = 1.28

Inboard row

	x/c, %	
L.S.	1.3	-0.334
	0.86	-0.281
	0	Inoperative
U.S.	0.73	0.313
	1.20	0.247
	3.30	0.099
	6.20	-0.001
	8.20	-0.044
	10.20	-0.068
	12.60	-0.122
	15.10	-0.163
	17.50	-0.205
	20.10	-0.211
	25.00	-0.211
	29.80	-0.250

Outboard row

	x/c, %	
L.S.	1.50	-0.429
	1.00	-0.458
	0	0.530
	1.00	0.347
	1.40	0.285
	3.60	0.172
	7.00	0.068
	9.10	0.022
	11.30	-0.007
	14.00	-0.058
	16.80	-0.100
	19.60	-0.117
	22.40	Inoperative
	22.70	-0.155
	33.00	-0.200

M = 1.458 Hp = 46,414 α = 5.46

Inboard row

	x/c, %	
L.S.	1.3	0.193
	0.86	0.153
	0	Inoperative
U.S.	0.73	0.037
	1.20	-0.021
	3.30	-0.138
	6.20	-0.213
	8.20	-0.258
	10.20	-0.282
	12.60	-0.325
	15.10	-0.337
	17.50	-0.358
	20.10	-0.353
	25.00	-0.351
	29.80	-0.434

Outboard row

	x/c, %	
L.S.	1.50	-0.245
	1.00	-0.323
	0	0.520
U.S.	1.00	0.124
	1.40	0.069
	3.60	-0.049
	7.00	-0.126
	9.10	-0.159
	11.30	-0.208
	14.00	-0.238
	16.80	-0.267
	19.60	-0.281
	22.40	Inoperative
	22.70	-0.341
	33.00	-0.371

M = 1.798 Hp = 54,651 α = 1.04

Inboard row

	x/c, %	
L.S.	1.3	-0.229
	0.86	-0.179
	0	Inoperative
U.S.	0.73	0.423
	1.20	0.343
	3.30	0.204
	6.20	0.111
	8.20	0.056
	10.20	0.044
	12.60	-0.011
	15.10	-0.066
	17.50	-0.110
	20.10	-0.118
	25.00	-0.122
	29.80	-0.161

Outboard row

	x/c, %	
L.S.	1.50	-0.317
	1.00	-0.319
	0	0.578
	1.00	0.441
	1.40	0.380
	3.60	0.275
	7.00	0.178
	9.10	0.124
	11.30	0.075
	14.00	0.035
	16.80	-0.007
	19.60	-0.028
	22.40	Inoperative
	22.70	-0.066
	33.00	-0.095

M = 1.759 Hp = 54,100 α = 7.64

Inboard row

	x/c, %	
L.S.	1.3	0.239
	0.86	0.228
	0	Inoperative
U.S.	0.73	0.156
	1.20	0.096
	3.30	-0.009
	6.20	-0.080
	8.20	-0.128
	10.20	-0.161
	12.60	-0.187
	15.10	-0.230
	17.50	-0.244
	20.10	-0.242
	25.00	-0.223
	29.80	-0.294

Outboard row

	x/c, %	
L.S.	1.50	-0.098
	1.00	-0.160
	0	0.585
U.S.	1.00	0.215
	1.40	0.153
	3.60	0.048
	7.00	-0.025
	9.10	-0.062
	11.30	-0.090
	14.00	-0.132
	16.80	-0.161
	19.60	-0.175
	22.40	Inoperative
	22.70	-0.219
	33.00	-0.245

M = 1.796 Hp = 49,029 α = 2.03

Inboard row

	x/c, %	
L.S.	1.3	-0.197
	0.86	-0.157
	0	Inoperative
U.S.	0.73	0.407
	1.20	0.344
	3.30	0.194
	6.20	0.100
	8.20	0.049
	10.20	0.021
	12.60	-0.008
	15.10	-0.054
	17.50	-0.096
	20.10	-0.116
	25.00	-0.110
	29.80	-0.164

Outboard row

	x/c, %	
L.S.	1.50	-0.301
	1.00	-0.299
	0	0.598
U.S.	1.00	0.430
	1.40	0.384
	3.60	0.274
	7.00	0.169
	9.10	0.118
	11.30	0.084
	14.00	0.039
	16.80	-0.003
	19.60	-0.022
	22.40	Inoperative
	22.70	-0.066
	33.00	-0.104

M = 1.732 Hp = 49,166 α = 4.51

Inboard row

	x/c, %	
L.S.	1.3	-0.116
	0.86	-0.058
	0	Inoperative
U.S.	0.73	0.316
	1.20	0.248
	3.30	0.109
	6.20	0.015
	8.20	-0.030
	10.20	-0.060
	12.60	-0.095
	15.10	-0.115
	17.50	-0.154
	20.10	-0.174
	25.00	-0.202
	29.80	-0.223

Outboard row

	x/c, %	
L.S.	1.50	-0.259
	1.00	-0.270
	0	0.609
U.S.	1.00	0.347
	1.40	0.299
	3.60	0.189
	7.00	0.085
	9.10	0.025
	11.30	0.009
	14.00	-0.033
	16.80	-0.067
	19.60	-0.093
	22.40	Inoperative
	22.70	-0.136
	33.00	-0.161

M = 0.898 Hp = 39,662 α = 3.33
With notch-bump

Inboard row

	x/c, %	
L.S.	1.3	-0.110
	0.86	-0.133
	0	Inoperative
U.S.	0.73	-0.319
	1.20	-0.415
	3.30	-0.582
	6.20	-0.577
	8.20	-0.650
	10.20	-0.689
	12.60	-0.709
	15.10	-0.625
	17.50	-0.558
	20.10	-0.554
	25.00	-0.538
	29.80	-0.669

Outboard row

	x/c, %	
L.S.	1.50	-0.506
	1.00	-0.493
	0	0.342
U.S.	1.00	-0.213
	1.40	-0.297
	3.60	-0.406
	7.00	-0.562
	9.10	-0.599
	11.30	-0.576
	14.00	-0.595
	16.80	-0.644
	19.60	-0.660
	22.40	Inoperative
	22.70	-0.653
	33.00	-0.718

M = 0.882 Hp = 39,331 α = 7.32
With notch-bump

Inboard row

	x/c, %	
L.S.	1.3	0.268
	0.86	0.320
	0	Inoperative
U.S.	0.73	-1.315
	1.20	-1.315
	3.30	-1.258
	6.20	-1.314
	8.20	-1.330
	10.20	-1.354
	12.60	-1.357
	15.10	-1.410
	17.50	-1.411
	20.10	-1.422
	25.00	-1.311
	29.80	-1.404

Outboard row

	x/c, %	
L.S.	1.50	0.146
	1.00	0.217
	0	-0.498
U.S.	1.00	-1.138
	1.40	-1.195
	3.60	-1.266
	7.00	-1.318
	9.10	-1.349
	11.30	-1.327
	14.00	-1.316
	16.80	-1.382
	19.60	-1.342
	22.40	Inoperative
	22.70	-1.009
	33.00	-0.966

M = 1.193 Hp = 47,108 α = 2.88
With notch-bump

Inboard row

	x/c, %	
L.S.	1.3	-0.344
	0.86	-0.392
	0	Inoperative
U.S.	0.73	0.098
	1.20	0.007
	3.30	-0.159
	6.20	-0.243
	8.20	-0.306
	10.20	-0.301
	12.60	-0.355
	15.10	-0.411
	17.50	-0.450
	20.10	-0.493
	25.00	-0.436
	29.80	-0.484

Outboard row

	x/c, %	
L.S.	1.50	-0.327
	1.00	-0.310
	0	0.480
U.S.	1.00	0.159
	1.40	0.094
	3.60	-0.030
	7.00	-0.163
	9.10	-0.240
	11.30	-0.263
	14.00	-0.311
	16.80	-0.327
	19.60	-0.325
	22.40	Inoperative
	22.70	-0.408
	33.00	-0.467

M = 1.157 Hp = 45,380 α = 8.60
With notch-bump

Inboard row

	x/c, %	
L.S.	1.3	0.325
	0.86	0.353
	0	Inoperative
U.S.	0.73	-0.432
	1.20	-0.459
	3.30	-0.571
	6.20	-0.633
	8.20	-0.645
	10.20	-0.675
	12.60	-0.702
	15.10	-0.737
	17.50	-0.776
	20.10	-0.773
	25.00	-0.703
	29.80	-0.783

Outboard row

	x/c, %	
L.S.	1.50	0.163
	1.00	0.181
	0	0.235
U.S.	1.00	-0.329
	1.40	-0.392
	3.60	-0.506
	7.00	-0.554
	9.10	-0.594
	11.30	-0.622
	14.00	-0.640
	16.80	-0.664
	19.60	-0.670
	22.40	Inoperative
	22.70	-0.722
	33.00	-0.756

M = 1.472 Hp = 50,311 α = 1.81
With notch-bump

Inboard row

	x/c, %	
L.S.	1.3	-0.201
	0.86	-0.218
	0	Inoperative
U.S.	0.73	0.281
	1.20	0.209
	3.30	0.059
	6.20	-0.038
	8.20	-0.082
	10.20	-0.097
	12.60	-0.129
	15.10	-0.174
	17.50	-0.226
	20.10	-0.243
	25.00	-0.238
	29.80	-0.265

Outboard row

	x/c, %	
L.S.	1.50	-0.174
	1.00	-0.170
	0	0.553
U.S.	1.00	0.327
	1.40	0.270
	3.60	0.167
	7.00	0.044
	9.10	0.004
	11.30	-0.047
	14.00	-0.089
	16.80	-0.131
	19.60	-0.143
	22.40	Inoperative
	22.70	-0.207
	33.00	-0.243

M = 1.405 Hp = 50,765 α = 8.18
With notch-bump

Inboard row

	x/c, %	
L.S.	1.3	0.334
	0.86	0.364
	0	Inoperative
U.S.	0.73	-0.137
	1.20	-0.185
	3.30	-0.298
	6.20	-0.353
	8.20	-0.383
	10.20	-0.405
	12.60	-0.434
	15.10	-0.467
	17.50	-0.483
	20.10	-0.493
	25.00	-0.447
	29.80	-0.486

Outboard row

	x/c, %	
L.S.	1.50	0.181
	1.00	0.147
	0	0.429
U.S.	1.00	-0.048
	1.40	-0.123
	3.60	-0.227
	7.00	-0.275
	9.10	-0.322
	11.30	-0.340
	14.00	-0.373
	16.80	-0.395
	19.60	-0.409
	22.40	Inoperative
	22.70	-0.445
	33.00	-0.480

M = 1.669 Hp = 54,508 α = 7.94
With notch-bump

Inboard row

	x/c, %	
L.S.	1.3	0.262
	0.86	0.297
	0	Inoperative
U.S.	0.73	0.072
	1.20	0.017
	3.30	-0.101
	6.20	-0.157
	8.20	-0.200
	10.20	-0.223
	12.60	-0.257
	15.10	-0.283
	17.50	-0.308
	20.10	-0.310
	25.00	-0.275
	29.80	-0.346

Outboard row

	x/c, %	
L.S.	1.50	0.041
	1.00	0.017
	0	0.533
U.S.	1.00	0.116
	1.40	0.091
	3.60	-0.028
	7.00	-0.093
	9.10	-0.129
	11.30	-0.171
	14.00	-0.186
	16.80	-0.233
	19.60	-0.258
	22.40	Inoperative
	22.70	-0.271
	33.00	-0.291

M = 1.715 Hp = 54,577 α = 1.30
With notch-bump

Inboard row

	x/c, %	
L.S.	1.3	-0.288
	0.86	-0.224
	0	Inoperative
U.S.	0.73	0.344
	1.20	0.277
	3.30	0.130
	6.20	0.047
	8.20	-0.019
	10.20	-0.032
	12.60	-0.058
	15.10	-0.127
	17.50	-0.153
	20.10	-0.176
	25.00	-0.179
	29.80	-0.218

Outboard row

	x/c, %	
L.S.	1.50	-0.381
	1.00	-0.395
	0	0.526
U.S.	1.00	0.373
	1.40	0.313
	3.60	0.212
	7.00	0.101
	9.10	0.055
	11.30	0.027
	14.00	-0.029
	16.80	-0.071
	19.60	-0.090
	22.40	Inoperative
	22.70	-0.140
	33.00	-0.172

M = 1.193 Hp = 41,931 α = 1.09
With notch-bump

Inboard row

	x/c, %	
L.S.	1.3	-0.436
	0.86	-0.495
	0	Inoperative
U.S.	0.73	0.188
	1.20	0.115
	3.30	-0.047
	6.20	-0.131
	8.20	-0.200
	10.20	-0.229
	12.60	-0.281
	15.10	-0.329
	17.50	-0.346
	20.10	-0.349
	25.00	-0.339
	29.80	-0.367

Outboard row

	x/c, %	
L.S.	1.50	-0.367
	1.00	-0.364
	0	0.445
U.S.	1.00	0.260
	1.40	0.192
	3.60	0.062
	7.00	-0.077
	9.10	-0.137
	11.30	-0.180
	14.00	-0.232
	16.80	-0.274
	19.60	-0.287
	22.40	Inoperative
	22.70	-0.352
	33.00	-0.369

M = 1.182 Hp = 41.533 α = 5.24
With notch-bump

Inboard row

	x/c, %	
L.S.	1.3	0.136
	0.86	0.137
	0	Inoperative
U.S.	0.73	-0.134
	1.20	-0.240
	3.30	-0.372
	6.20	-0.412
	8.20	-0.469
	10.20	-0.479
	12.60	-0.501
	15.10	-0.551
	17.50	-0.540
	20.10	-0.570
	25.00	-0.563
	29.80	-0.637

Outboard row

	x/c, %	
L.S.	1.50	-0.209
	1.00	-0.215
	0	0.451
U.S.	1.00	-0.067
	1.40	-0.101
	3.60	-0.214
	7.00	-0.332
	9.10	-0.404
	11.30	-0.445
	14.00	-0.456
	16.80	-0.509
	19.60	-0.494
	22.40	Inoperative
	22.70	-0.545
	33.00	-0.577

M = 1.493 Hp = 47,021 α = 1.11
With notch-bump

Inboard row

	x/c, %	
L.S.	1.3	-0.235
	0.86	-0.270
	0	Inoperative
U.S.	0.73	0.345
	1.20	0.259
	3.30	0.117
	6.20	0.011
	8.20	-0.035
	10.20	-0.056
	12.60	-0.102
	15.10	-0.156
	17.50	-0.202
	20.10	-0.208
	25.00	-0.213
	29.80	-0.247

Outboard row

	x/c, %	
L.S.	1.50	-0.204
	1.00	-0.217
	0	0.549
U.S.	1.00	0.367
	1.40	0.309
	3.60	0.200
	7.00	0.081
	9.10	0.028
	11.30	-0.010
	14.00	-0.041
	16.80	-0.092
	19.60	-0.118
	22.40	Inoperative
	22.70	-0.167
	33.00	-0.205

M = 1.478 Hp = 46,098 α = 5.57
With notch-bump

Inboard row

	x/c, %	
L.S.	1.3	0.181
	0.86	0.186
	0	Inoperative
U.S.	0.73	0.062
	1.20	0.011
	3.30	-0.101
	6.20	-0.185
	8.20	-0.243
	10.20	-0.270
	12.60	-0.303
	15.10	-0.339
	17.50	-0.358
	20.10	-0.350
	25.00	-0.340
	29.80	-0.408

Outboard row

	x/c, %	
L.S.	1.50	-0.227
	1.00	-0.271
	0	0.511
U.S.	1.00	0.127
	1.40	0.063
	3.60	-0.035
	7.00	-0.121
	9.10	-0.164
	11.30	-0.203
	14.00	-0.236
	16.80	-0.267
	19.60	-0.313
	22.40	Inoperative
	22.70	-0.327
	33.00	-0.352

REFERENCES

Banner, R.D.; McTigue, J.G.; and Petty, Gilbert, Jr.: Boundary-Layer Transition in Full-Scale Flight. NACA Conference on High-Speed Aerodynamics, Mar. 1958.

Chiles, H.R.; and Johnson, J.B.: Development of a Temperature-Compensated Hot-Film Anemometer System for Boundary-Layer Transition Detection on High-Performance Aircraft. NASA TM-86732, 1985.

Fisher, D.F.; and Dougherty, N.S., Jr.: In-Flight Transition Measurement on a 10° Cone at Mach Numbers From 0.5 to 2.0. NASA TP-1971, 1982.

Gaster, M: A Simple Device for Preventing Turbulent Contamination on Swept Leading Edges. Royal Aero. Soc. J. Technical Notes, vol. 69, Nov. 1965, pp. 788-789.

Holmes, B.J.; Gall, P.D.; Croom, C.C.; Manuel, G.S.; and Kelliher, W.C.: A New Method for Laminar Boundary Layer Transition Visualization in Flight — Color Changes in Liquid Crystal Coatings. NASA TM-87666, 1986.

McTigue, J.G.; Overton, J.D.; and Petty, Gilbert, Jr.: Two Techniques for Detecting Boundary-Layer Transition in Flight at Supersonic Speeds and at Altitudes Above 20,000 Feet. NASA TN D-18, 1959.

Meyer, R.R.; Trujillo, B.M.; and Bartlett, D.W.: F-14 VSTFE and Results of the Cleanup Flight Test Program. Presented at Research in Natural Laminar Flow and Laminar-Flow Control Symposium, Langley Research Center, Hampton, Virginia, Mar. 1987. NASA CP-2487, Part 2, 1987.

Runyan, L.J.; Navran, B.H.; and Rozendaal, R.A.: F-111 Natural Laminar Flow Glove Flight Test Data Analysis and Boundary Layer Stability Analysis. NASA CR-166051, 1984.

TABLE 1. — F-15 AIRFOIL COORDINATES
Butt line (BL) 160 in.

Upper surface		Lower surface	
x/c	z/c	x/c	z/c
0.00000000	0.00000000	0.00000000	0.00000000
0.00059247	0.00204976	0.00140765	-0.00159829
0.00223626	0.00415909	0.00376388	-0.00281839
0.00415688	0.00503680	0.00584315	-0.00282515
0.00888825	0.00761491	0.01111231	-0.00330331
0.02854337	0.01469216	0.03145677	-0.00300669
0.04855364	0.01979557	0.05144643	-0.00218559
0.09894502	0.02850951	0.10105463	-0.00095231
0.14937433	0.03381859	0.15062629	-0.00103670
0.19967105	0.03716926	0.20032923	-0.00184030
0.24982642	0.03931962	0.25017399	-0.00278309
0.29987906	0.04068059	0.30012100	-0.00347595
0.34988075	0.04145605	0.35011938	-0.00371327
0.39987320	0.04172819	0.40012700	-0.00343121
0.44988255	0.04151548	0.45011780	-0.00266167
0.49991540	0.04081573	0.50008453	-0.00148894
0.54996425	0.03963478	0.55003582	-0.00001655
0.60001482	0.03800423	0.59998531	0.00165827
0.65005312	0.03598742	0.64994708	0.00346009
0.70007212	0.03367442	0.69992774	0.00533976
0.75007340	0.03116691	0.74992654	0.00726948
0.80006502	0.02855171	0.79993498	0.00922871
0.85005878	0.02586397	0.84994095	0.01117663
0.90006005	0.02303923	0.89993974	0.01301631
0.95005843	0.01985590	0.94994184	0.01454806
0.98004020	0.01759840	0.97995980	0.01517715
0.99002727	0.01675709	0.98997252	0.01531408
1.00000000	0.01564020	1.00000000	0.01564020

TABLE 1. — Continued.

BL 190

Upper surface		Lower surface	
x/c	z/c	x/c	z/c
0.00000000	0.00000000	0.00000000	0.00000000
0.00067135	0.00156582	0.00132907	-0.00106342
0.00236780	0.00332090	0.00363288	-0.00182660
0.00427904	0.00422124	0.00572149	-0.00175277
0.00900515	0.00672067	0.01099542	-0.00188968
0.02852992	0.01425356	0.03147031	-0.00095004
0.04840646	0.02008026	0.05159383	0.00030198
0.09859657	0.03057650	0.10140343	0.00270596
0.14896463	0.03729205	0.15103566	0.00401942
0.19927878	0.04163773	0.20072172	0.00467128
0.24949614	0.04444756	0.25050465	0.00505683
0.29963588	0.04622552	0.30036462	0.00543685
0.34973020	0.04725856	0.35027050	0.00594808
0.39980801	0.04769324	0.40019257	0.00663941
0.44988623	0.04758969	0.45011455	0.00750201
0.49996751	0.04696607	0.50003299	0.00850168
0.55004672	0.04582800	0.54995349	0.00959863
0.60011338	0.04419414	0.59988662	0.01076437
0.65015840	0.04210338	0.64984139	0.01198460
0.70017766	0.03962178	0.69982283	0.01325794
0.75017323	0.03683325	0.74982698	0.01458428
0.80015425	0.03382498	0.79984624	0.01594316
0.85013115	0.03066279	0.84986905	0.01726522
0.90010962	0.02735675	0.89989087	0.01839107
0.95008305	0.02381999	0.94991674	0.01902732
0.98005690	0.02149488	0.97994303	0.01897901
0.99004480	0.02066853	0.98995512	0.01885944
1.00000000	0.01924987	1.00000000	0.01924987

TABLE 1. — Concluded.

BL 210

Upper surface		Lower surface	
x/c	z/c	x/c	z/c
0.00000000	0.00000000	0.00000000	0.00000000
0.00064038	0.00168623	0.00135993	-0.00118319
0.00231698	0.00351105	0.00368273	-0.00201224
0.00423460	0.00437767	0.00576508	-0.00189731
0.00896232	0.00684125	0.01103770	-0.00196541
0.02850404	0.01416007	0.03149631	-0.00049245
0.04837015	0.01989854	0.05162958	0.00141087
0.09846401	0.03079307	0.10153612	0.00549372
0.14873490	0.03846843	0.15126439	0.00831183
0.19900694	0.04397168	0.20099323	0.01018376
0.24923596	0.04789334	0.25076404	0.01149391
0.29942119	0.05060329	0.30057854	0.01253994
0.34957334	0.05233683	0.35042737	0.01351731
0.39970335	0.05324466	0.40029652	0.01453549
0.44981991	0.05342474	0.45017969	0.01563694
0.49992665	0.05294707	0.50007335	0.01682052
0.55002118	0.05186946	0.54997864	0.01805579
0.60009874	0.05025124	0.59990140	0.01930069
0.65015540	0.04815602	0.64984456	0.02050916
0.70018880	0.04565582	0.69981157	0.02163780
0.75019882	0.04282512	0.74980118	0.02264740
0.80019082	0.03973165	0.79980958	0.02349829
0.85017003	0.03642500	0.84983010	0.02414459
0.90013943	0.03291567	0.89986053	0.02451810
0.95009594	0.02915301	0.94990385	0.02451409
0.98005892	0.02671957	0.97994075	0.02426400
0.99004401	0.02586887	0.98995607	0.02412866
1.00000000	0.02448176	1.00000000	0.02448176

TABLE 2. — CHORDWISE PRESSURE ORIFICE LOCATIONS

Identification no.		Inboard row, % (C = 137.3 in.)	Outboard row, % (C = 99.4 in.)
L.S.	1	1.3	1.5
	2	0.86	1.0
	3	0*	0
U.S.	4	0.73	1.0
	5	1.2	1.4
	6	3.3	3.6
	7	6.2	7.0
	8	8.2	9.1
	9	10.2	11.3
	10	12.6	14.0
	11	15.1	16.8
	12	17.5	19.6
	13	20.1	22.4*
	14	25.0	27.7
	15	29.8	33.0

*Pressure orifice inoperative.

TABLE 3. — HOT-FILM SENSOR LOCATIONS

Flight no.	Location (% chord)				
	No.1, outboard	No. 2	No. 3	No. 4	No. 5, inboard
463	5	10	15	20	25
464	5	10	15	20	15
465	5	10	15	20	15
466	5	10	15	20	15
467	5	10	15	20	15
468	0	2	4	10	15
469	1	2	4	10	15
470	1	2	4	10	15
471	1	2	4	10	15

Figure 1. In-flight photograph of F-15 aircraft with foam and fiberglass test section.

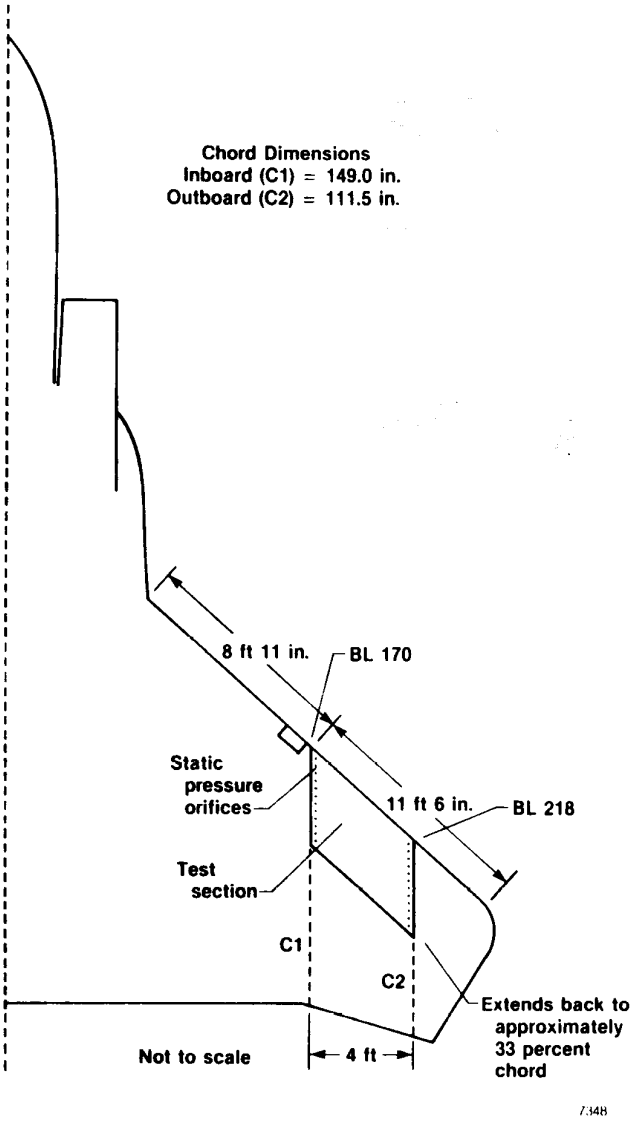

Figure 2. Location of foam and fiberglass test section.

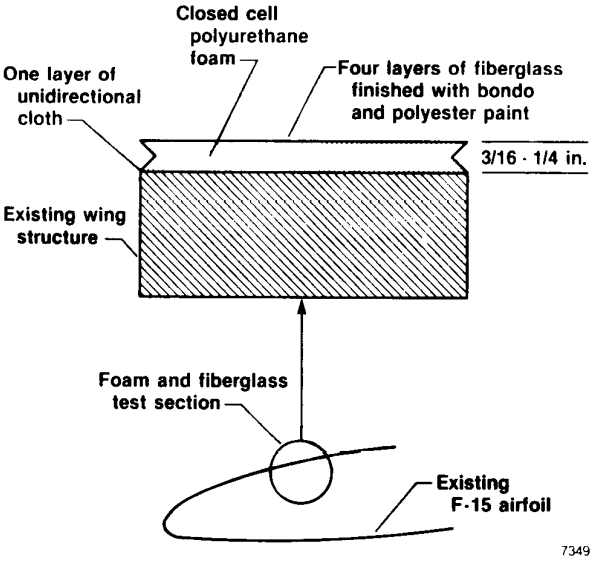

Figure 3. Schematic of F-15 aircraft test section construction.

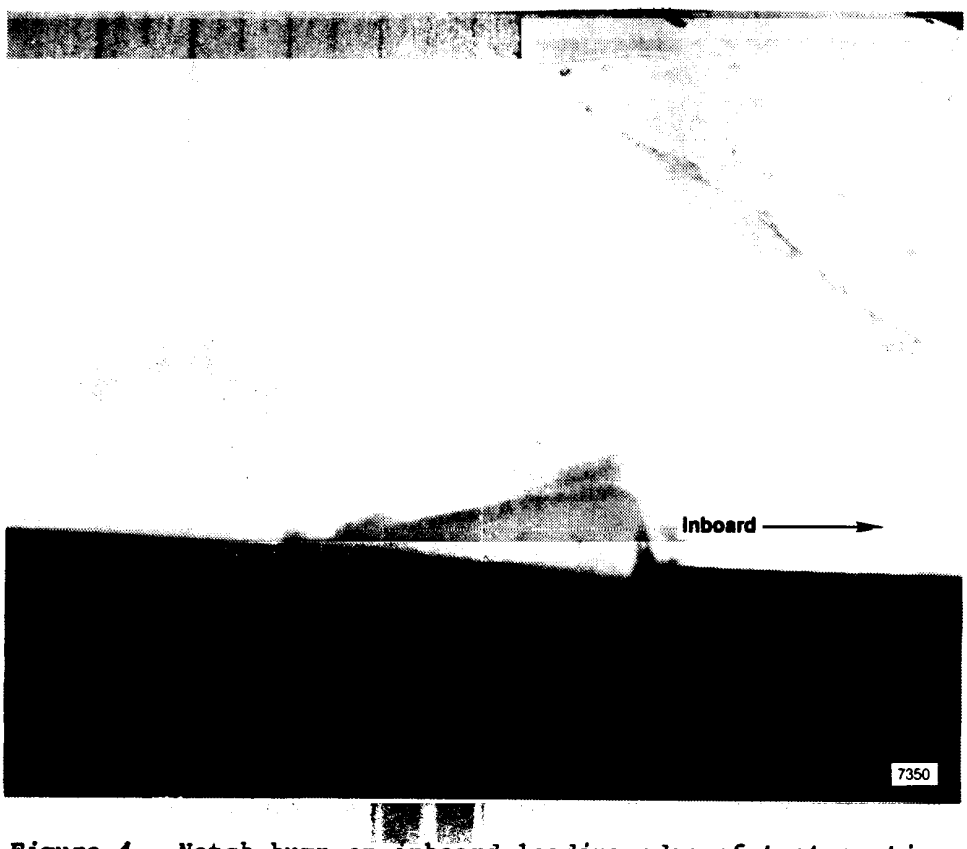

Figure 4. Notch-bump on inboard leading edge of test section.

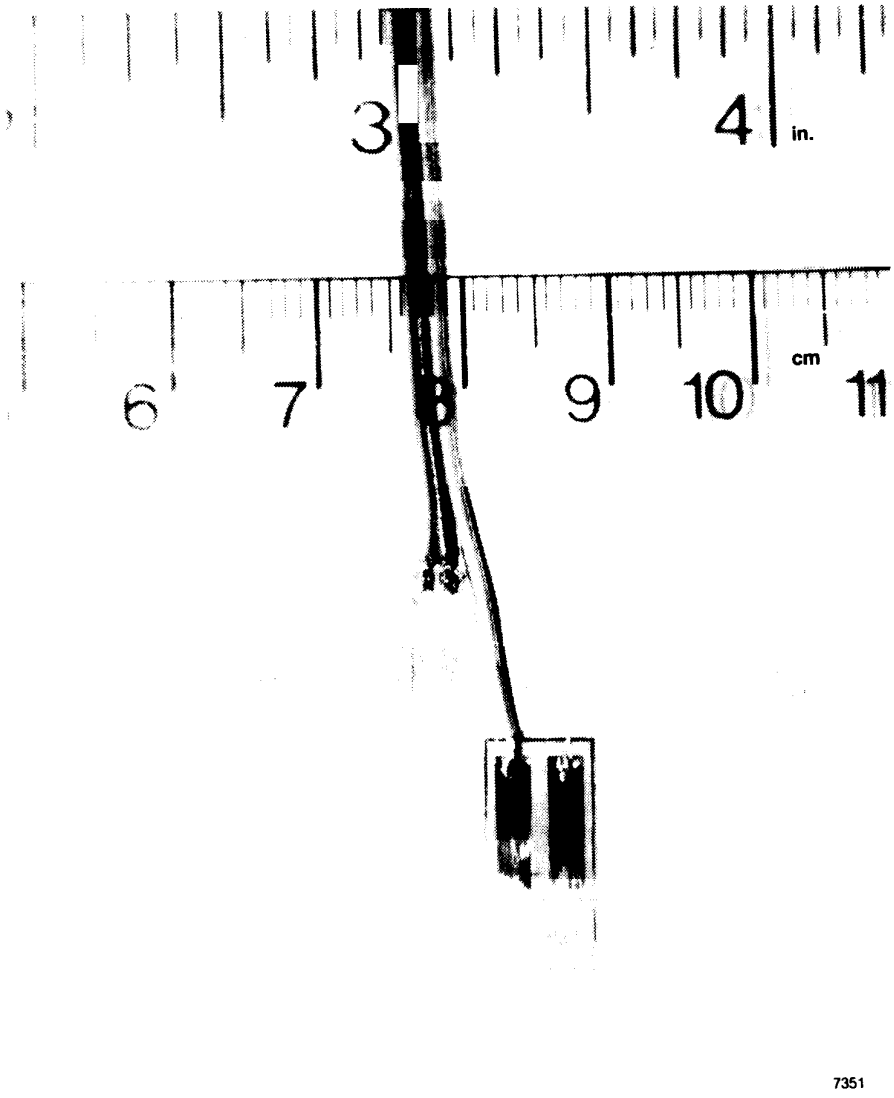

Figure 5. Closeup of typical hot-film sensor and temperature gage installation.

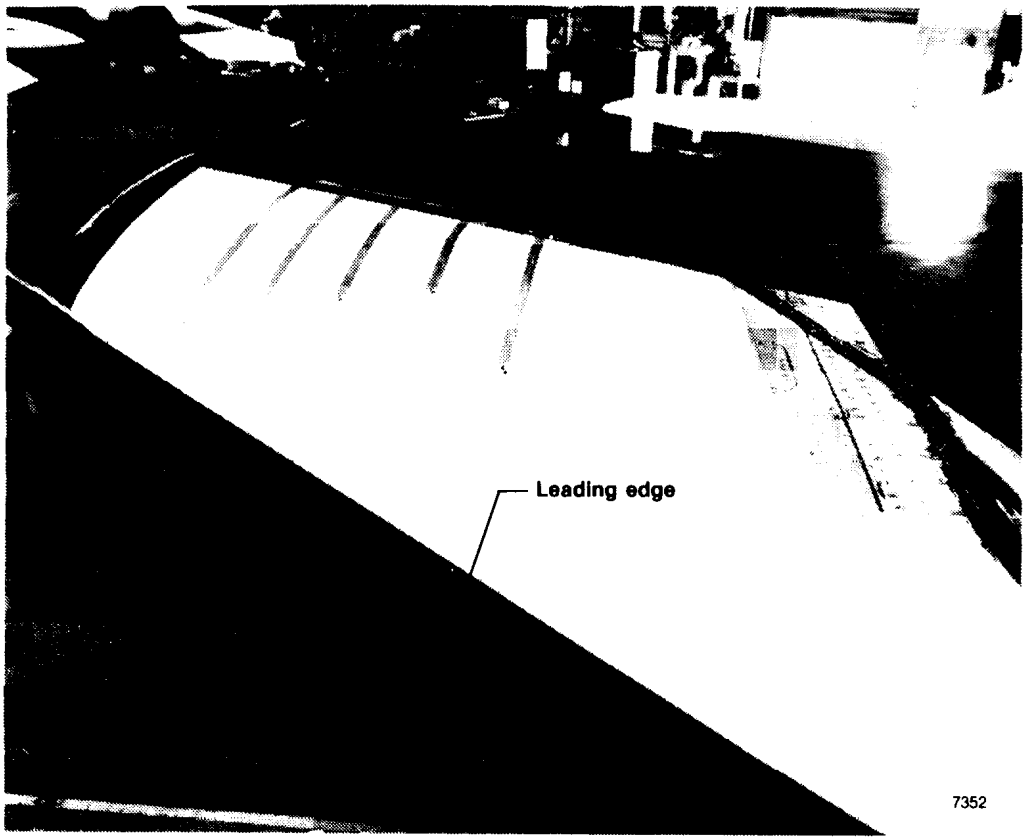

Figure 6. Hot-film sensors mounted on test section prior to notch-bump installation.

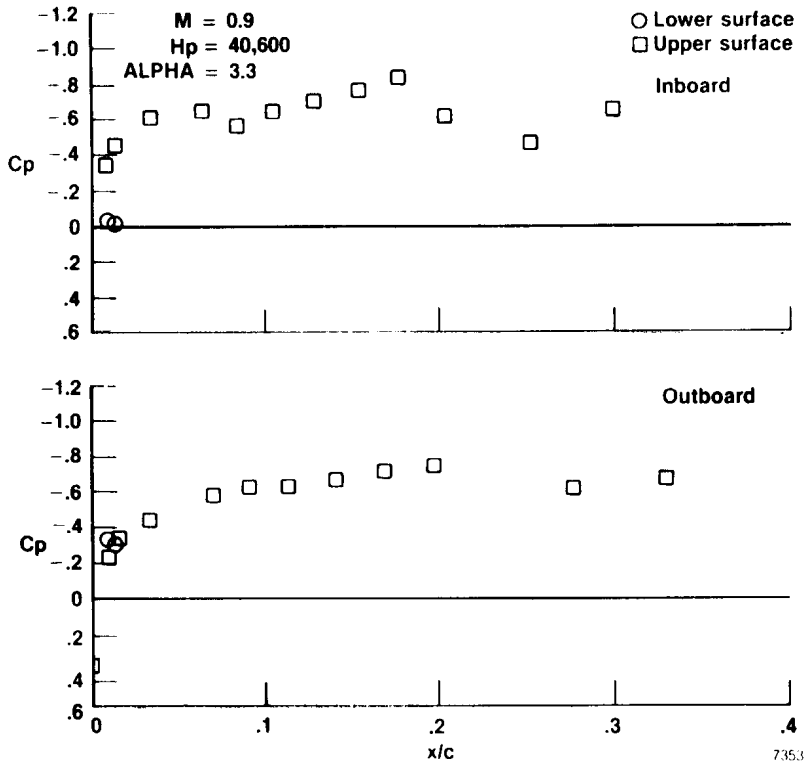

(a)

Figure 7. Typical pressure distributions.

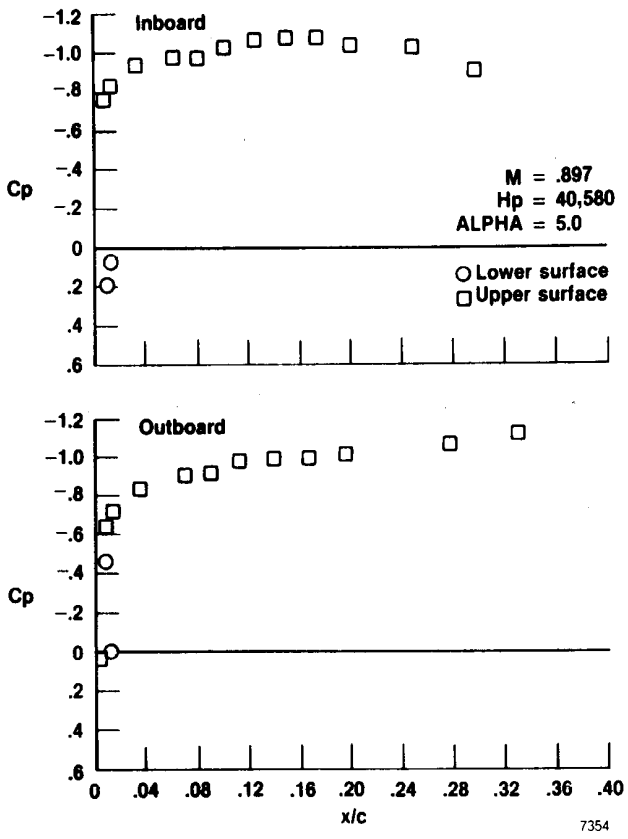

(b)

Figure 7. Continued.

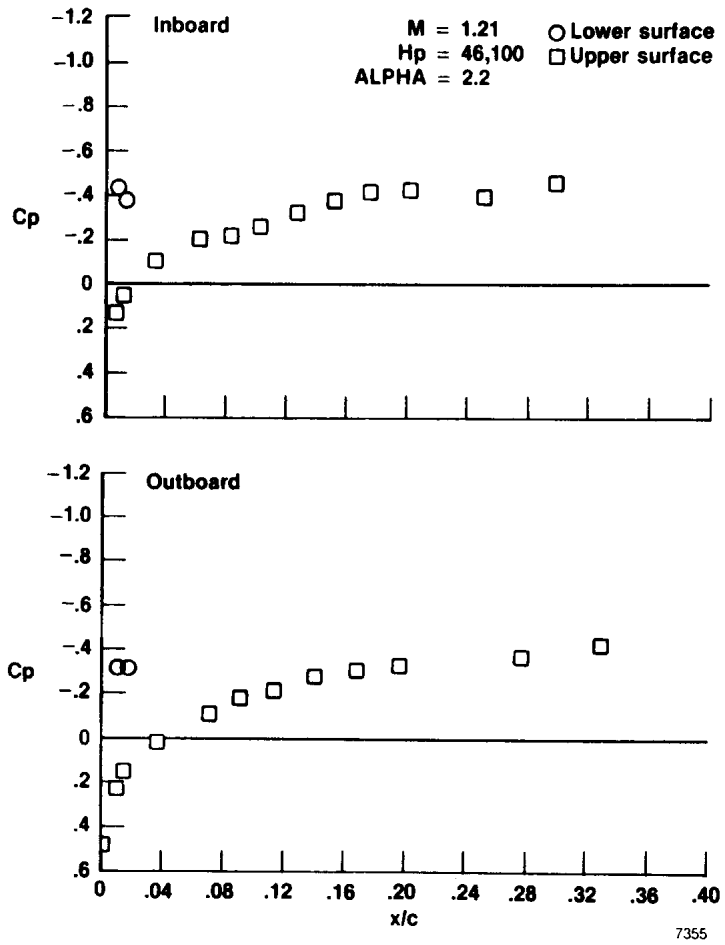

(c)

Figure 7. Continued.

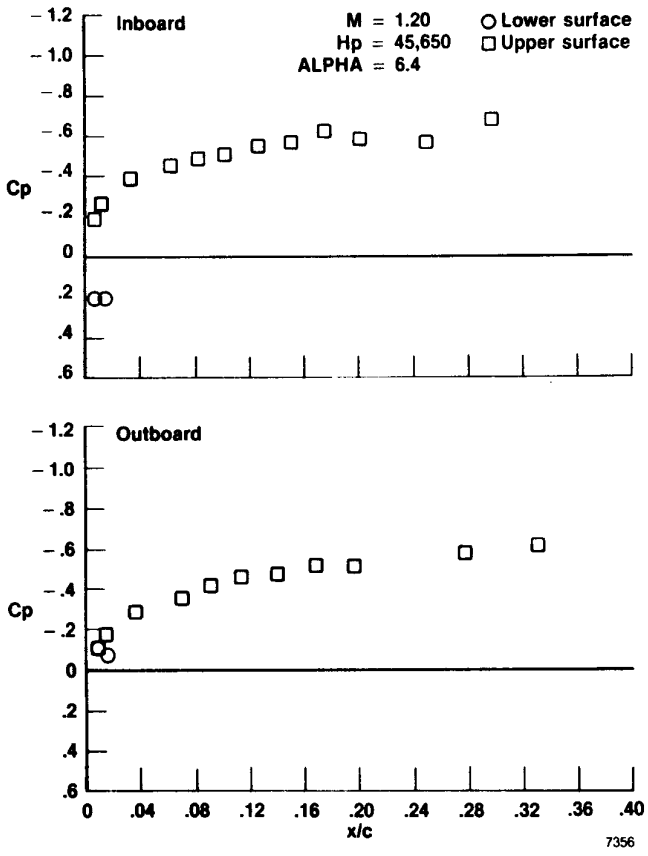

(d)

Figure 7. Continued.

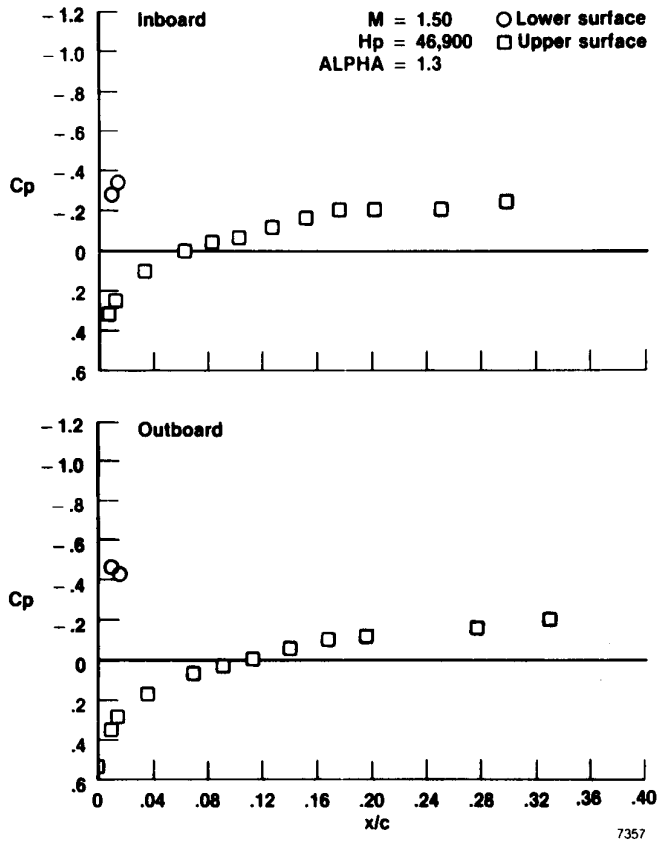

(e)

Figure 7. Continued.

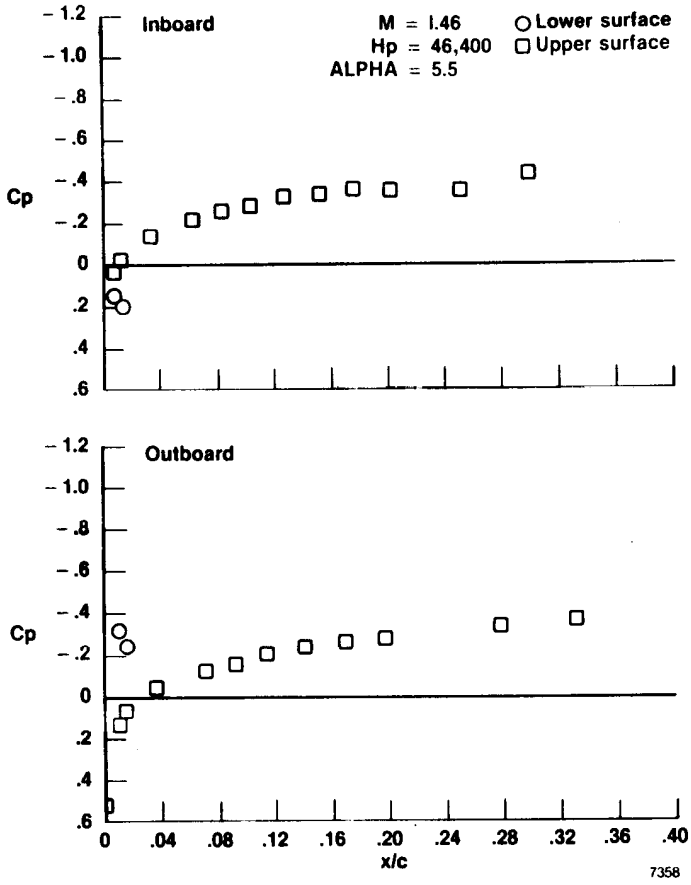

(f)

Figure 7. Continued.

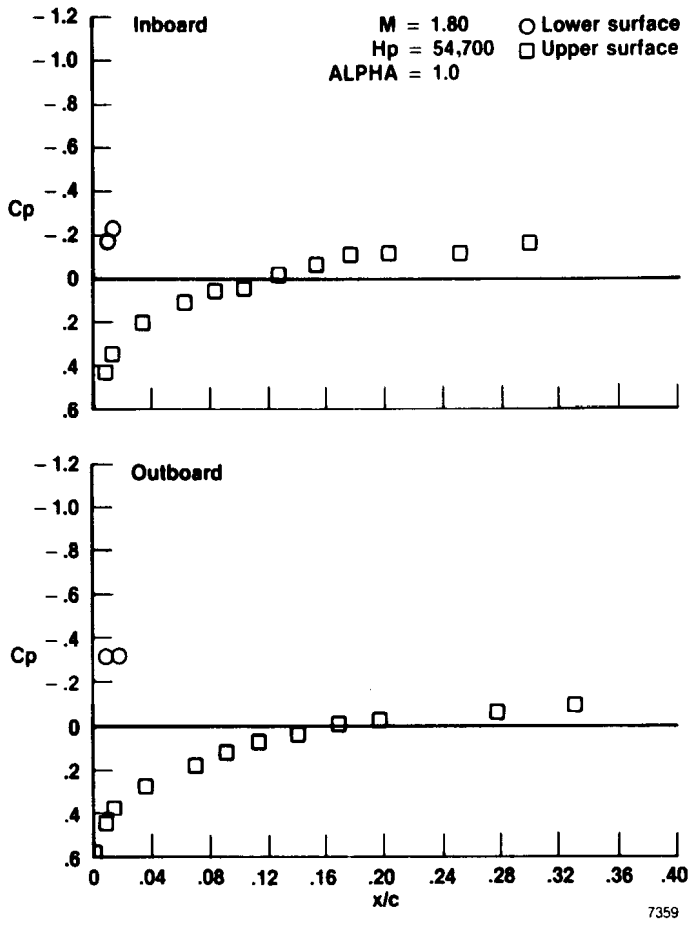

(g)

Figure 7. Continued.

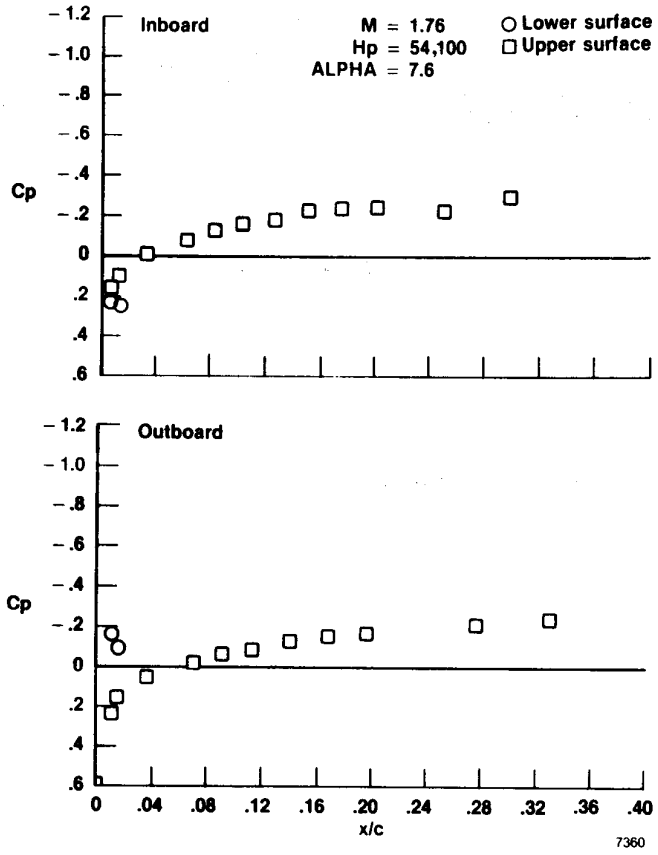

(h)

Figure 7. Concluded.

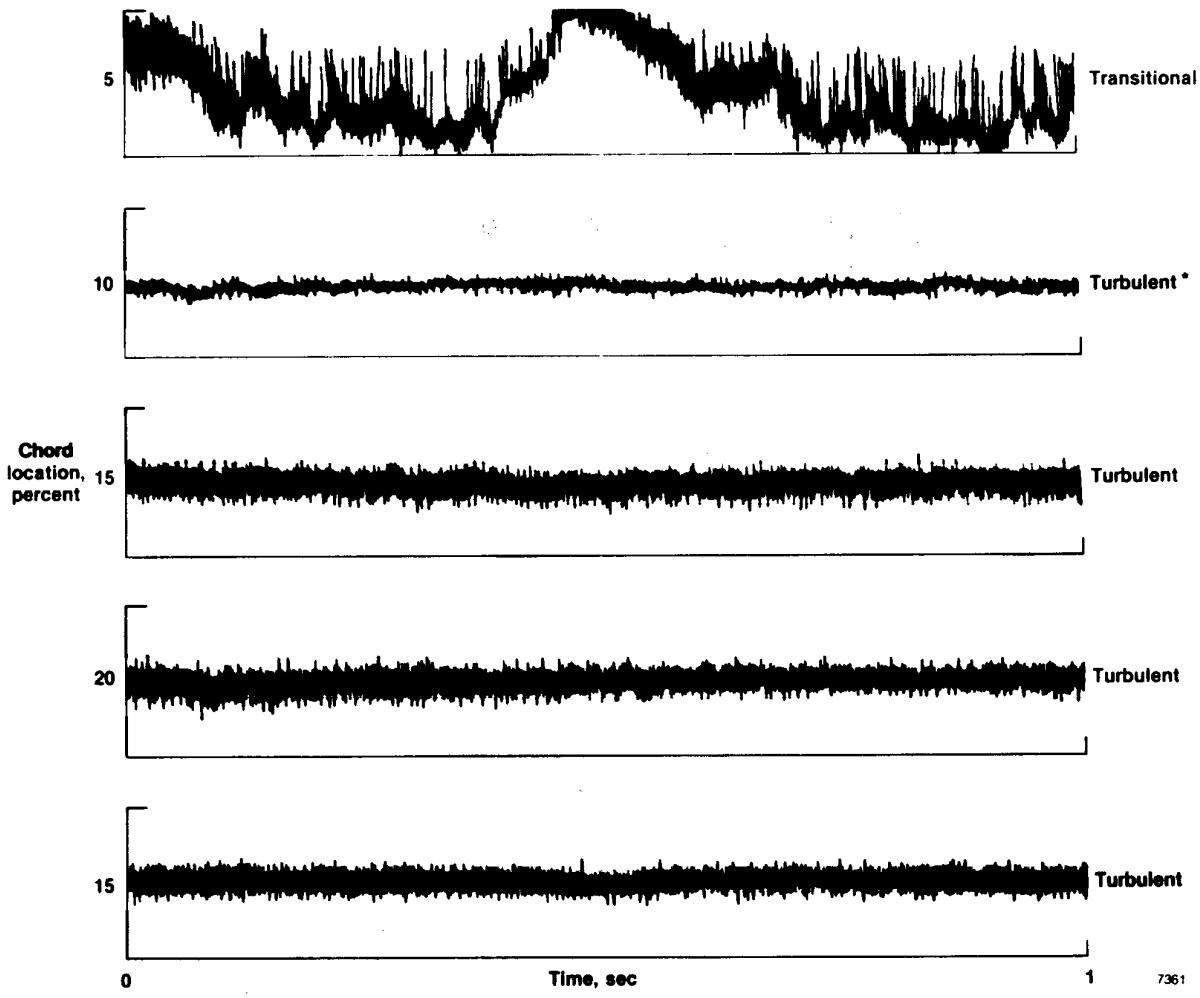

*(a) Alpha = 3.3°; *low-gain setting.*

Figure 8. Typical hot-film output. M = 0.9, Hp = 40,600 ft.

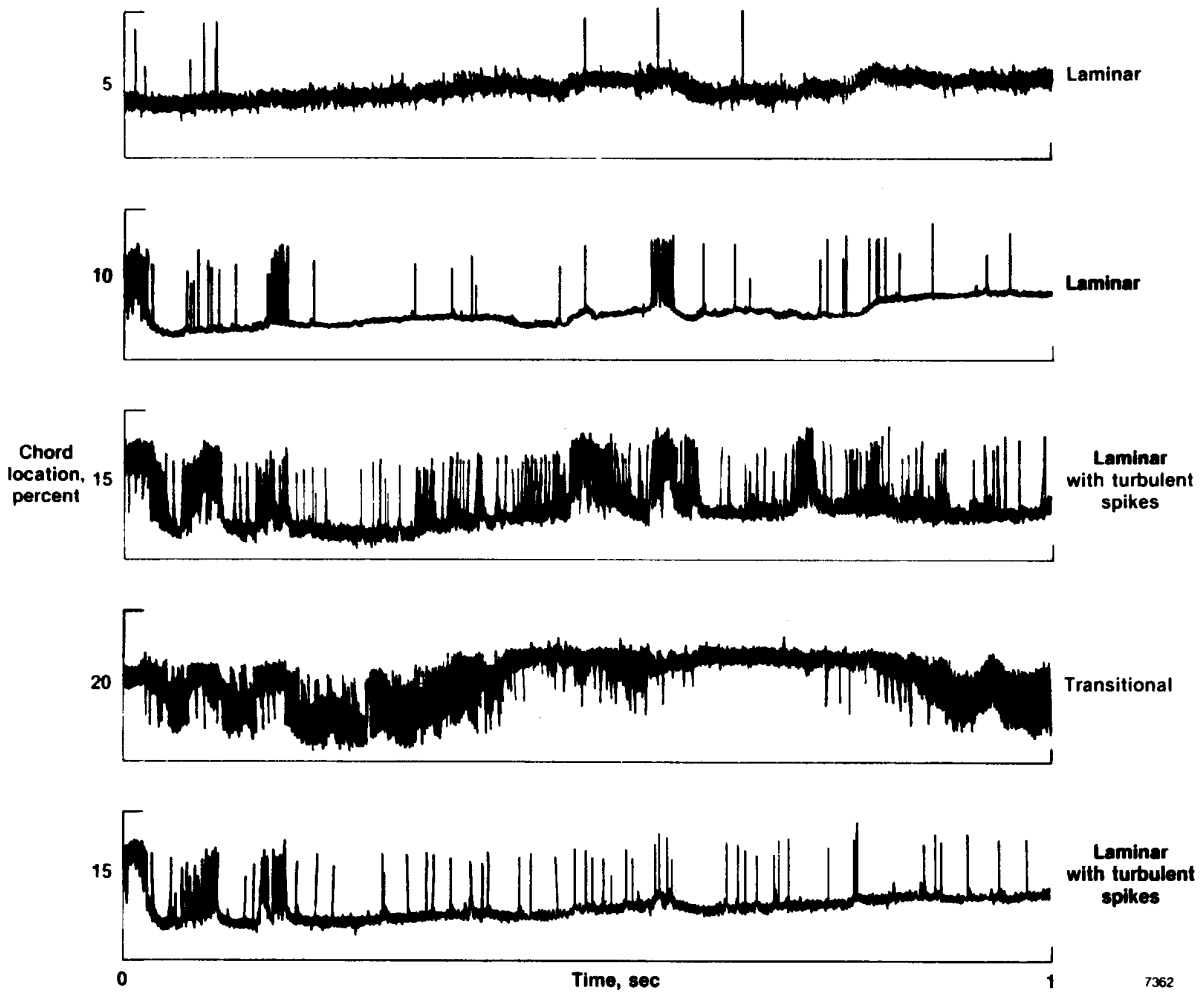

(b) Alpha = 5.0°.

Figure 8. Concluded.

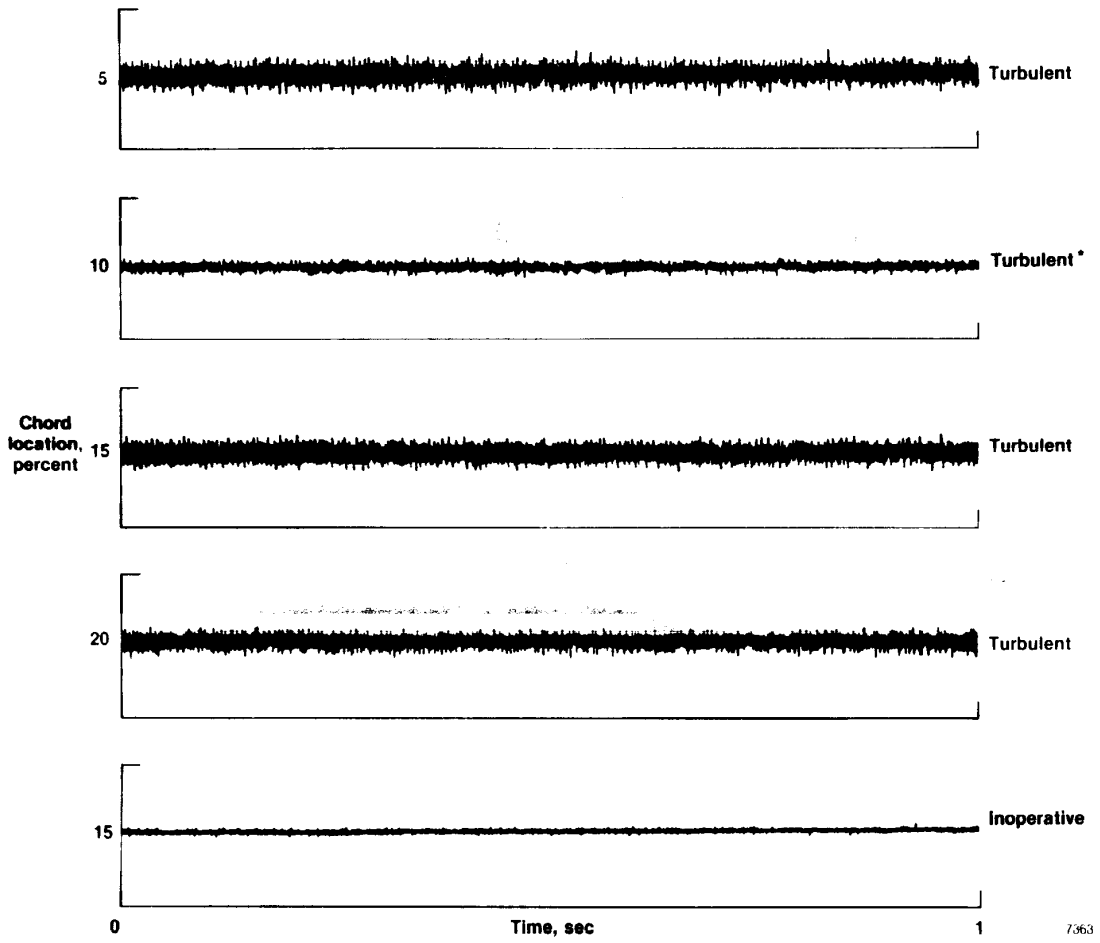

Figure 9. Typical hot-film output. M = 1.73, Hp = 49,200 ft, α = 4.5°.

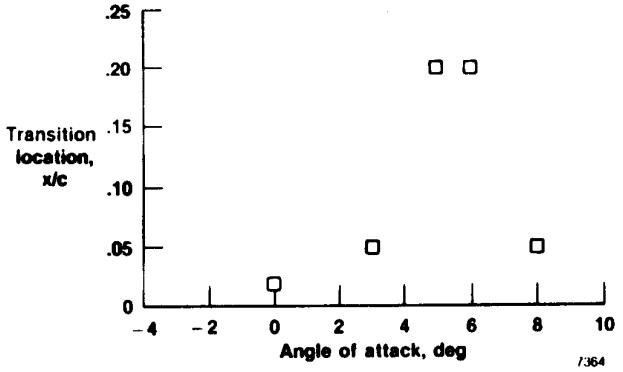

Figure 10. Optimum transition location as a function of angle of attack. Clean configuration. M = 0.9, Hp = 40,000 ft.

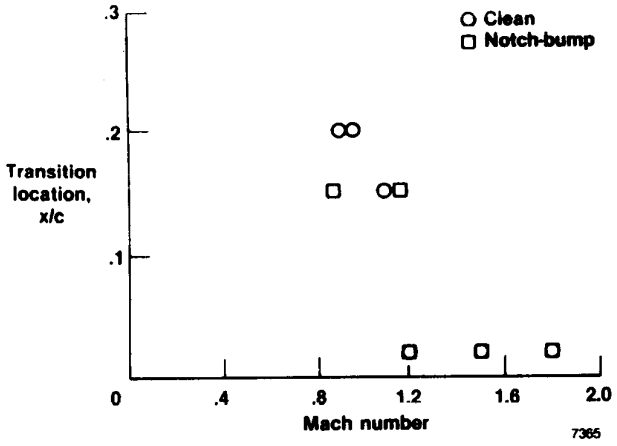

Figure 11. Optimum transition location as a function of Mach number.

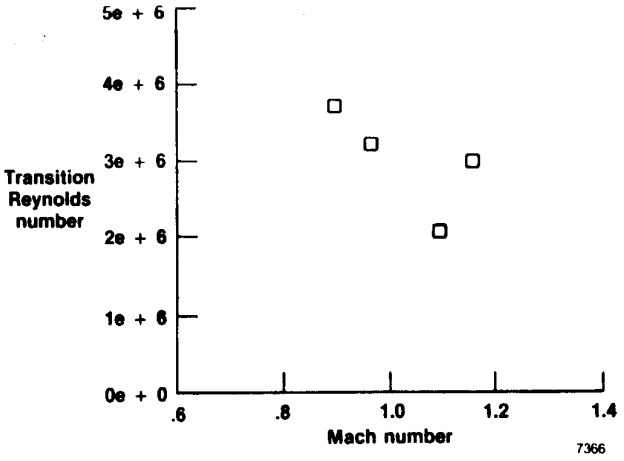

Figure 12. Transition Reynolds number as a function of Mach number.

NASA National Aeronautics and Space Administration

Report Documentation Page

1. Report No.	2. Government Accession No.	3. Recipient's Catalog No.
NASA TM-100412		

4. Title and Subtitle	5. Report Date
Preliminary In-Flight Boundary Layer Transition Measurements on a 45-Degree Swept Wing at Mach Numbers Between 0.9 and 1.8	March 1988
	6. Performing Organization Code
7. Author(s)	8. Performing Organization Report No.
J. Blair Johnson	H-1436
	10. Work Unit No.
	RTOP 533-02-21
9. Performing Organization Name and Address	11. Contract or Grant No.
NASA Ames Research Center Dryden Flight Research Facility P.O. Box 273 Edwards, CA 93523-5000	
12. Sponsoring Agency Name and Address	13. Type of Report and Period Covered
National Aeronautics and Space Administration Washington, DC 20546	Technical Memorandum
	14. Sponsoring Agency Code

15. Supplementary Notes

16. Abstract

A preliminary flight experiment was flown to generate a full-scale supersonic data base to aid the assessment of computational codes, to improve instrumentation for measuring boundary layer transition at supersonic speeds, and to provide preliminary information for the definition of follow-on programs. The experiment was conducted using an F-15 aircraft that was modified with a small cleanup test section on the right wing. Results are presented for Mach (M) numbers from 0.9 to 1.8 at altitudes from 26,000 to 55,000 ft. At $M > 1.2$, transition occurred near or at the leading edge for the clean configuration. The furthest aft that transition was measured was 20 percent chord at $M = 0.9$ and $M = 0.97$. No change in transition location was observed after the addition of a notch-bump on the leading edge of the inboard side of the test section which was intended to minimize attachment line transition problems. Some flow visualization was attempted during the flight experiment with both subliming chemicals and liquid crystals. However, difficulties arose from the limited time the test aircraft was able to hold test conditions and the difficulty of positioning the photo chase aircraft during supersonic test points. Therefore, no supersonic transition results were obtained using flow visualization.

17. Key Words (Suggested by Author(s))	18. Distribution Statement
Supersonic laminar flow Laminar flow Natural laminar flow	Unclassified — Unlimited Subject category 34

19. Security Classif. (of this report)	20. Security Classif. (of this page)	21. No. of pages	22. Price
Unclassified	Unclassified	45	A03